

Finite-Element Stress Analysis of a Multicomponent Model of Sheared and Focally-Adhered Endothelial Cells

MICHAEL C. FERKO, AMIT BHATNAGAR, MARIANA B. GARCIA, and PETER J. BUTLER

Department of Bioengineering, The Pennsylvania State University, 205 Hallowell Building, University Park, PA 16802, USA

(Received 3 April 2006; accepted 23 October 2006; published online: 12 December 2006)

Abstract—Hemodynamic forces applied at the apical surface of vascular endothelial cells may be redistributed to and amplified at remote intracellular organelles and protein complexes where they are transduced to biochemical signals. In this study we sought to quantify the effects of cellular material inhomogeneities and discrete attachment points on intracellular stresses resulting from physiological fluid flow. Steady-state shear- and magnetic bead-induced stress, strain, and displacement distributions were determined from finite-element stress analysis of a cell-specific, multicomponent elastic continuum model developed from multimodal fluorescence images of confluent endothelial cell (EC) monolayers and their nuclei. Focal adhesion locations and areas were determined from quantitative total internal reflection fluorescence microscopy and verified using green fluorescence protein–focal adhesion kinase (GFP–FAK). The model predicts that shear stress induces small heterogeneous deformations of the endothelial cell cytoplasm on the order of < 100 nm. However, strain and stress were amplified 10–100-fold over apical values in and around the high-modulus nucleus and near focal adhesions (FAs) and stress distributions depended on flow direction. The presence of a $0.4 \mu\text{m}$ glycocalyx was predicted to increase intracellular stresses by ~ 2 -fold. The model of magnetic bead twisting rheometry also predicted heterogeneous stress, strain, and displacement fields resulting from material heterogeneities and FAs. Thus, large differences in moduli between the nucleus and cytoplasm and the juxtaposition of constrained regions (e.g. FAs) and unattached regions provide two mechanisms of stress amplification in sheared endothelial cells. Such phenomena may play a role in subcellular localization of early mechanotransduction events.

Keywords—Cell mechanics, Endothelial cells, Total internal reflection, Focal adhesions, Mechanotransduction, Continuum, Elastic, Glycocalyx, Focal adhesion kinase.

INTRODUCTION

The endothelium is a primary regulator of vascular health and derangement of this system can lead to

diseases such as atherosclerosis. It is subject to hemodynamic forces (e.g. shear stress, τ) which depend on the location in the vasculature, the heart rate, and the metabolic demands of tissues. Endothelial cells (ECs) are sensitive to temporal shear gradients^{5,6,17} and spatial shear gradients,¹⁴ the nature of which is thought to determine whether ECs exhibit an atherogenic or atheroprotective phenotype.³⁷ Shear stress also plays a major role in the coordination of blood flow in the microvasculature^{6,31} and, hence, in the maintenance of capillary blood pressure, and the delivery of oxygen, nutrients and immunity-related leucocytes to the tissue.

The precise mechanisms by which apical shear stress leads to localized intracellular signaling remains unknown but may involve three possible general mechanisms. First, shear stress may directly perturb a cellular structure which is directly linked to a diffusible factor leading to downstream intracellular biochemical signaling. For example, shear stress activates G-proteins which are coupled directly to the membrane.²¹ Second, cellular architecture may redistribute apically applied forces to intracellular organelles where forces induce signaling locally. For example, stress fibers connected to the apical membrane may distribute stress to remote cellular locations and activate stress-fiber-associated proteins there.⁵⁴ Third, shear stress may induce a combination of these effects in which biochemical signals are initiated at the apical surface, a diffusible activating factor is generated, and propagation and focusing of this signal is facilitated by local forces. There is strong evidence for this third model. First, shear-induced nitric oxide production depends on an intact glycocalyx^{16,36} and shear causes increases in EC-membrane lipid lateral diffusion⁴ and free volume,²² suggesting shear stresses are directly “felt” by the apical surface of the cell which includes the glycocalyx and plasma membrane. In support of decentralized forces, shear stress caused deformation of intermediate filaments,²³ strain focusing at focal adhesions (FAs)²⁴ and stress focusing in the cell interior.²⁵ But shear stress also

Address correspondence to Peter J. Butler, Department of Bioengineering, The Pennsylvania State University, 228 Hallowell Building, University Park, PA 16802, USA. Electronic mail: pbutler@psu.edu

activates PECAM-1, a protein in cell junctions near the cell surface. This activation may lead to production of a diffusible factor which induces activation of integrins in FAs, where stresses may be concentrated.⁵² Local potentiation of cell signaling by forces are suggested by studies in which endothelial cells actively reorganize their points of attachment, (e.g. FAs), and align them in the direction of flow.^{12,56} Directional reorientation of FAs may be due to a combination of integrin activation and forces which bias the location of new integrin-extracellular matrix bonds. In support of this idea, shear-induced shc-integrin association (thought to be responsible for activation of various mitogen activated protein kinases) was dependent on new integrin binding to the extracellular matrix.²⁷ Shear stress also leads to polarized adaptive changes in cell mechanics.^{44,45} Taken together, such studies support a model of cellular mechanotransduction in which the global activation of signaling pathways by shear-forces are converted to local signaling events in discrete locations in cells by force amplification and force-induced directional biasing of signal propagation. Thus, there is a need for models which quantify how the unique architecture of endothelial cells can amplify forces from shear stress at discrete cellular locations.

Constitutive mechanical continuum models predict deformation and stresses in subcellular structures of cells in response to force applications. These models use average values of mechanical constants which arise from complex cellular architecture. Experimentally applied forces and readouts of deformation suggest that cell responses to stress can be modeled using linear elasticity,⁸ tensegrity,⁵³ poroelasticity,¹⁰ viscoelasticity,³⁰ power-law rheology,³² and scale-free glassy rheology³ depending on the magnitude and mode of force application. Finite element analysis remains the most effective tool to apply these constitutive frameworks to complex loading protocols and geometries; a process which is necessary in order to assess cellular responses to forces on multiple spatial and temporal scales. For example, Mack and colleagues recently used finite element analysis to assess force transmission from the translation of embedded beads from the cell surface to FAs.³⁴ They found that finite element analysis of a continuum model which included a cortical membrane and viscoelastic cytoplasm was able to predict FA stress directions that correlated well with FA translocation.

Although there has been excellent progress in defining cell mechanics, most models do not include faithful reconstruction of subcellular topography or organelles, information which may be important in cell-specific responses to applied forces. In response to this challenge, we recently developed new integrated methods in fluorescence imaging and image processing for the development of solid models with cell-specific

topographies and subcellular organelles.¹⁵ The goal of the present study was to use these methodologies along with total internal reflection fluorescence microscopy (TIRFM) to create a cell-specific, multicomponent, three-dimensional solid elastic continuum model of an endothelial cell in a confluent monolayer with experimentally determined FAs. Finite element analysis was used to compute stress transmission throughout the endothelial cell due to fluid flow or magnetic bead twisting applied at the apical surface. It is possible that juxtaposition of high and low moduli organelles and constrained and unconstrained regions are two mechanisms of stress amplification in cells. Thus, we quantified the effects of FAs and material inhomogeneity on deformation, strain, and stress distributions in the cell interior. In order to compare our model with available experimental data, we computed stresses and displacements at 1 μm above the cell base in response to magnetic bead twisting as in Ref. 25. In the discussion, we estimate the degree of stress amplification due to the presence of an intact glycocalyx. This type of cell-specific modeling based on experimentally-determined topographies and boundary conditions may help identify potential sites of force-induced potentiation and directional-biasing of cell signaling.

MATERIALS AND METHODS

Cell Culture, Staining, and Transfection of GFP-FAK

Bovine aortic endothelial cells (BAECs), passages 2–10, were grown to confluence (~2–3 days) on a #1 chambered-coverslip (Labtek, Campbell, CA) in Dulbecco's modified eagle medium (DMEM) supplemented with 10% fetal calf serum (FCS), 2 mM L-glutamine, 100 Units/ml penicillin and streptomycin (BioSource, Camarillo, CA). The cytoplasm was stained with calcein-AM, and the nucleus was counterstained with Hoechst 33258 (Invitrogen, Carlsbad, CA). Imaging was performed on cells in phosphate buffered saline (PBS) + 1% albumin at room temperature. In separate experiments, cells were transfected with plasmids encoding for green fluorescence protein–focal adhesion kinase (GFP-FAK) using lipofectamine transfection protocols and counterstained with calcein-AM-orange.

3-D Imaging

Cells on coverslips were mounted on a piezoelectric z-stage (Mad City Labs, Inc., Madison, WI), and viewed on an Olympus IX71 fluorescence microscope using xenon arc lamp illumination, a PlanApo 60x/1.45 NA TIRFM oil-immersion objective (Olympus, Japan), and a Sensicam QE CCD camera (Cooke Corp.,

Romulus, MI). In order to minimize photobleaching, a TTL-modulated shutter (Uniblitz, Inc., Rochester, NY) was used to match illumination and image exposure times through a custom LabVIEW program and an A/D board (National Instruments, Austin, TX). The axial slice spacing was $0.2 \mu\text{m}$ per image representing a slight over-sampling as determined by the Rayleigh depth of field. The total z -sampling distance was twice the full apparent depth of the object. Exposure time was adjusted such that peak grayscale values were 80% of the maximum bin value for the camera.

Empirical Axial Distortion Correction

The axial spacing of 2-D images in a 3-D image stack must be adjusted to account for axial distortions that accompany imaging through media with different indices of refraction. 3-D data sets of cells with unknown axial dimensions were corrected using an axial distortion correction function (ADCF) as described previously.¹⁵ Briefly, an empirical, non-linear ADCF was developed from 3-D image stacks of $15 \mu\text{m}$ fluorescent microspheres (Invitrogen, Carlsbad, CA). This correction function converts equal axial spacing of microsphere and cell images to non-equal spacing such that, in 3-dimensions, the microsphere has equal radii in all directions. This procedure minimizes axial distortions in the cell image which arise from spherical aberrations and refractive index mismatches.

Quantitative Total Internal Reflection Fluorescence Microscopy

Focal adhesions of the cultured calcein-stained BAECs and GFP-FAK transfected cells were viewed with objective-based total internal reflection fluorescence microscopy (TIRFM) (Olympus, Lehigh, PA) with a tunable krypton-argon ion laser (Melles Griot, Carlsbad, CA). Laser light was transmitted to the system via fiber optic and corresponding coupling system (Point-source, Hamble, Southampton, England). TIRFM images were processed with 2-D adaptive blind deconvolution (Autoquant, Albany, NY) to reduce blur and attenuate intensity gradients across the image plane. Deconvolution had a negligible effect on the quantitation of FA size and area.⁴⁷

TIRFM images were taken on the same cell and region of interest as the 3-D image sets. The distance of an excited fluorophore from the coverglass $[\Delta(x,y)]$ is given by:⁵¹

$$\Delta(x,y) = \Delta_0 + d_p \ln[F_0/F(x,y)] \quad (1)$$

where Δ_0 is the minimum separation distance (10 nm), F_0 is the maximum image intensity corresponding to fluorophores exactly at the minimum separation

distance, and $F(x,y)$ is pixel intensity. d_p is the depth of penetration of an evanescent wave due to a totally reflected light beam and is given by:

$$d_p(\theta_i) = \lambda/[4\pi n_{\text{eff}}[\sin^2(\theta_i) - (n_{\text{eff}}/n_g)^2]^{1/2}] \quad (2)$$

where, θ_i is the incident angle of illumination, λ is the wavelength of excitation light, n_g is the index of refraction of glass (1.5), and n_{eff} is the effective refractive index of the sample (1.3). Illumination angle (73.15°) was determined through a linear interpolation between the critical angle (TIR first achieved) and the maximum angle for TIR of the objective (angle just before TIR was lost, based on the numerical aperture).

TIRF image intensities were converted to distances using Eqs. 1, 2 by a custom MATLAB program which rendered FAs into attachment points for the 3-D cell model. Binary arrays representing both focal contacts and close contacts were constructed by choosing a height threshold of 40 nm.³⁹ Focal adhesion borders were delineated by a 2-D spline function and the resulting 2-D object representing the FAs were embedded in the 3-D cell solid model (Fig. 1).

In separate experiments, GFP-FAK positive cells were stained with a red-shifted version of calcein-AM and imaged with TIRF using sequential excitation with 488 nm (for GFP) and 520 (for calcein-orange). The calcein images were analyzed for FAs as described above and colocalization software (ImageJ) was used to determine the degree to which FAs determined from the spline procedure colocalized with GFP-FAK-positive locations. Total colocalization, sizes, and areas of FAs determined from GFP-FAK and by quantitative TIRF were measured (Fig. 2).

Combined Multi-Component Model of Cell and Fluid Domains

After filtering and scaling with the ADCF, 3-D objects were converted to solid models. For geometries which contained complex and convoluted surfaces or internal features, solid models were created in MATLAB using a Qhull-based algorithm. To create models representing large-scale surface topographies, a custom ‘‘blanket rendering’’ algorithm was used.¹⁵ The complete cell model was then assembled from models for the nucleus, cell topography, and FAs and combined with a simulated flow field above the cell (Fig. 1D). This model was analyzed by finite element analysis (FEA) of extracellular flow and intracellular stress.

Finite Element Analysis of Fluid and Solid Domains

Assembly of fluid, solid (cell), and FA domains, automatic meshing, and all finite element analysis were

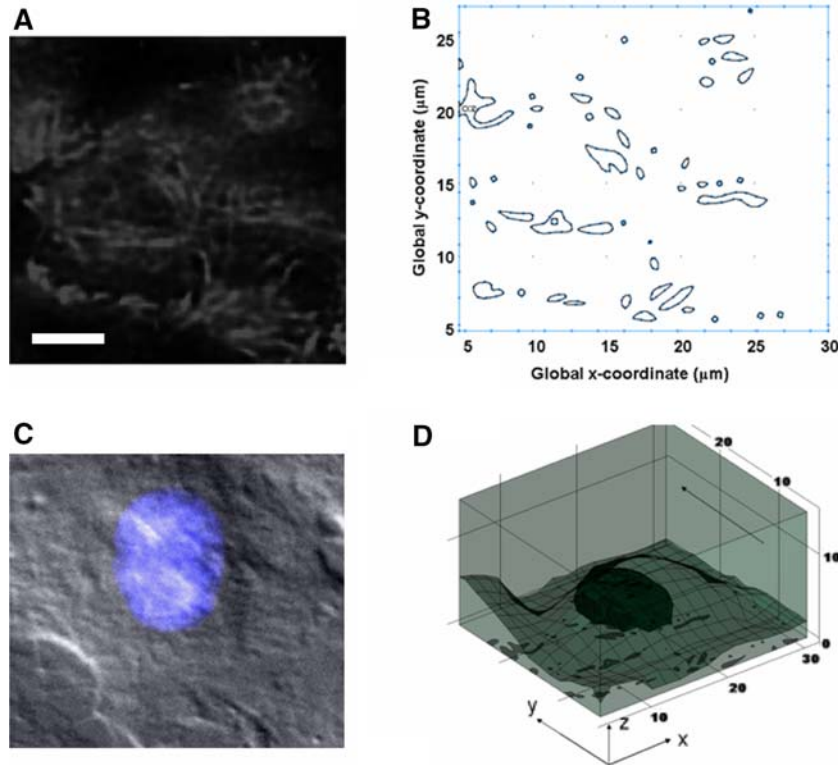


FIGURE 1. Solid modeling of cytoplasm, nucleus and focal adhesions. All images were obtained from the same cell on a multimodal microscope. (A) Image of calcein-stained cell (in a confluent monolayer) using TIRFM. Greater intensity indicates cell is closer to coverslip. Bar = 5 μm . (B) Resultant spline object created by the MATLAB program for quantitative TIRF. Intensities from 1A were converted to distance from coverslip using Eqs. 1, 2. Resulting image was thresholded at 40 nm from coverslip to model focal and close contacts. Result is a binary image indicating adhesion areas. (C) DIC image of cell monolayer with Hoestch-stained nucleus. (D) Multicomponent fluid–solid model: focal adhesions are outlined in black at the base of the model. The Qhull-rendered nucleus model is shown in dark green in the center. The cell monolayer is in light green. The flow field is above the monolayer. Direction of flow is in the positive y -direction (indicated by arrow). Axes in μm .

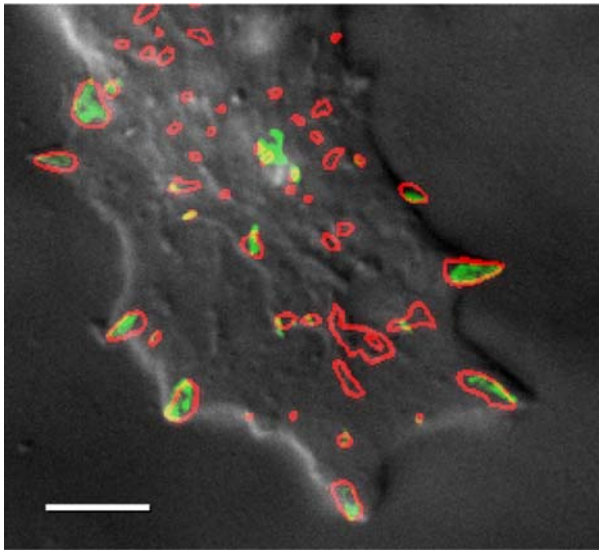


FIGURE 2. Colocalization of splined focal adhesions, GFP–FAK, and cell DIC image. Red splines and GFP–FAK fluorescence were superimposed on DIC image on sub-confluent endothelial cell. Bar = 5 μm .

performed using COMSOL Multiphysics software (COMSOL 3.2a, COMSOL Corp., Burlington, MA) on a Dell Computer (64-bit, 3.4 GHz, 12 GB RAM). The fluid velocity vector \mathbf{u} was modeled using the steady-state incompressible Navier–Stokes (NS) equation for Newtonian fluids according to:

$$\begin{aligned} \nabla p \mathbf{I} - \eta \nabla^2 \mathbf{u} + \rho (\mathbf{u} \cdot \nabla) \mathbf{u} &= 0 \\ \nabla \cdot \mathbf{u} &= 0 \end{aligned} \quad (3)$$

where \mathbf{I} is the identity matrix, η is dynamic viscosity (0.0084 poise), ρ is density, p is pressure, and body forces (e.g. gravity) are neglected. Total forces \mathbf{F}_T exerted on the cell surface by the fluid were computed from the velocity according to:

$$\mathbf{F}_T = -\mathbf{n} \cdot (-p \mathbf{I} + \eta (\nabla \mathbf{u} + (\nabla \mathbf{u})^T)) \quad (4)$$

where \mathbf{n} is a unit normal vector. This formulation for boundary forces accounts for viscous and normal forces (e.g. pressure). The relationship between the stress tensor, $\boldsymbol{\sigma}$, and strain, \mathbf{e} , for the cell cytoplasm and

nucleus was given by isotropic, linear elasticity theory according to:

$$\begin{aligned} \boldsymbol{\sigma} &= D\mathbf{e} + \boldsymbol{\sigma}_0 \\ D &= \frac{E}{(1+\nu)(1-2\nu)} \\ &\times \begin{bmatrix} 1-\nu & \nu & \nu & 0 & 0 & 0 \\ \nu & 1-\nu & \nu & 0 & 0 & 0 \\ \nu & \nu & 1-\nu & 0 & 0 & 0 \\ 0 & 0 & 0 & \frac{1-2\nu}{2} & 0 & 0 \\ 0 & 0 & 0 & 0 & \frac{1-2\nu}{2} & 0 \\ 0 & 0 & 0 & 0 & 0 & \frac{1-2\nu}{2} \end{bmatrix} \end{aligned} \quad (5)$$

with a Poisson's ratio, ν , of 0.33⁵⁰ and Young's moduli, E , of 775 and 1,500 Pa, for the cytoplasm and nucleus, respectively⁷ (Table 1) and an applied prestress, $\boldsymbol{\sigma}_0$. The total fluid stress tensor computed from Eq. 4 was applied to the cell surface as in.⁸ All stress components (σ_{ij}) were computed in the model and used to compute the von Mises stress (σ_{vM}), a stress invariant usually referred to as the effective stress. The von Mises stress (in the cell) was computed according to:

$$\sigma_{vM} = \left\{ \frac{1}{2} \left[(\sigma_{xx} - \sigma_{yy})^2 + (\sigma_{xx} - \sigma_{zz})^2 + (\sigma_{yy} - \sigma_{zz})^2 + 6(\sigma_{xy}^2 + \sigma_{xz}^2 + \sigma_{yz}^2) \right] \right\}^{1/2}. \quad (6)$$

Fluid Domain Boundary Settings

Pressure drop across the chamber (0.667 dynes/cm² per μm of channel length) was determined from a simplified finite element simulation of a channel without cells which produced a wall shear stress of 10 dynes/cm². The no-slip boundary condition was applied at the cell surface. The slip-symmetry boundary condition, defined such that there is no velocity component normal to the boundary and that

velocities inside and outside the boundary are equal, was applied to the tops and sides of the fluid domain (away from the cells). This boundary condition is consistent with the fact that the actual boundaries of the flow chamber are 100 s of microns away from the cell being simulated and, thus, will not influence the flow near the cell.

Solid Domain Boundary Settings

For the solid (cell) domain, the lateral edges of the simulation space were permitted to deform upon shear imposition, consistent with the observation that cells in a monolayer deform as a unit.²³ The total stress (shear and normal) from the fluid domain was applied to the cell surface by setting the surface force equal to the total boundary force derived from the incompressible Navier–Stokes equation (Eq. 4). Because deformations were small, the viscous stress tensor was not re-solved after cell deformation. When computing internal stresses resulting from FAs, boundaries corresponding to FAs were constrained in all three directions while the remaining cell base was free in the x - and y -directions and positive z -direction. To simulate cell stresses with a uniformly adhered base, both FAs and the remaining cell base were constrained in all directions. Thus, mesh parameters were identical for cells that were modeled as focally- or uniformly attached to the glass substrate. Similarly, mesh settings were identical for the cases in which the nucleus was present or absent by making the nuclear modulus equal to the true modulus or to the cytoplasm modulus, respectively.

Determination of Stress Focusing in Response to Shear Stress and Bead Twisting

Our model predicts that stresses can be concentrated (or focused) at discrete locations, even for distributed loads like shear stress. The only experimental data available that demonstrates stress focusing is by Hu *et al.* who analyzed mitochondria displacements in response to bead twisting.²⁵ In order to test whether our model could predict experimentally-observed stress focusing, we modified our finite element model to simulate bead twisting of 20° around the horizontal axis as in³⁵ and predicted the resultant deformation and stress distributions in the EC cytoplasm at 1 μm from the cell base. In this case fluid flow was not simulated over the cell surface.

Meshing, Solution Procedure, and Post-Processing

The combined solid models with material properties and boundary settings were meshed using tetrahedron

Table 1. Material properties used for simulation.

	E (Pa)	ν	ρ (g/cm ³)
<i>Cellular mechanical properties</i>			
Cell membrane + cytoplasm	775	0.33	1.25
Cell nucleus	5,100	0.33	1.25
<i>Extracellular fluid properties</i>			
	η (poise)	ρ (g/cm ³)	
DMEM	0.0084	1	

Mechanical properties are from Ref. 7. E is Young's modulus, ν is Poisson's ratio, ρ is density, and η is viscosity. Fluid properties are from Ref. 4.

elements. Meshes consisted of approximately 71,000 elements and approximately 420,000 degrees of freedom. The model was solved using a generalized non-linear solver and minimal residual (GMRES) iterative linear system solver. Simulations were performed on a Dell Xeon, 3.4 GHz 64-bit computer with 12 GB RAM. Sensitivity of the solution to different mesh parameters (e.g. coarseness) was evaluated. Computed stresses were found to be insensitive to changes in mesh parameters (data not shown). Post processing results for stresses, strains, and deformations were obtained using COMSOL post-processing features. Quantification of FA areas and numbers was performed using ImageJ particle-analysis tools.

RESULTS

GFP-FAK Fluorescence Colocalizes with Quantitative TIRFM of Calcein-Stained Cells

qTIRFM was used to detect FAs and focal contacts in calcein-stained cells by identifying where the membrane was within 40 nm of the coverglass. In order to determine whether these were mature FAs, in separate experiments on subconfluent cells, we imaged GFP-FAK-positive cells loaded with red-shifted calcein and computed areas where calcein-FAs were colocalized with GFP-FAK-positive regions. In these studies of five cells, $82 \pm 24\%$ (mean \pm SD) of FAs detected by quantitative TIRFM of calcein-stained cells were GFP-FAK-positive (data not shown) indicating that these were mature FAs (Fig. 2). The remaining 18% of attachment points detected by quantitative TIRF were comprised of small adhesion sites and represented

about 5% total FA area. Average areas of qTIRF-detected FAs and GFP-FAK-positive FAs in subconfluent cells were $0.69 \pm 0.56 \mu\text{m}^2$ and $0.56 \pm 0.51 \mu\text{m}^2$, respectively (not shown). In confluent cells, average qTIRF-detected FA area was $0.53 \pm 0.78 \mu\text{m}^2$. Thus, there was negligible difference between FA areas of newly adhered ECs and confluent ECs. A representative image in which splined FAs from quantitative TIRF and GFP-FAK-positive regions were superimposed on the DIC image is shown in Fig. 2.

Apical Shear Stress is Non-Uniform

Subcellular shear stress distributions from finite element analysis of AFM-rendered monolayers have been reported in the literature.² Consistent with these previous findings, in the present simulation of flow over fluorescence-rendered ECs, shear stress was non-uniform and depended on cell height (Fig. 3). Simulation on three cell monolayers resulted in non-uniform shear stress over the cell surface with a mean (\pm standard deviation) peak surface shear stress (τ_{max}) of $30.56 \pm 1.33 \text{ dynes/cm}^2$ which is consistent with values reported by Ref. 2. The overall mean shear was 10 dynes/cm^2 . All stress, strain, and deformation data reported in Figs. 3–5, 7–9 are derived from the representative model shown on Fig. 1.

Shear Stress Induces Heterogeneous Internal Cytoplasmic Deformations, Stresses, and Strains in Focally Adhered Endothelial Cells

The cell solid models predicted deformations in response to simulated fluid flow with a nominal surface shear stress of 10 dynes/cm^2 . Introduction of FAs as

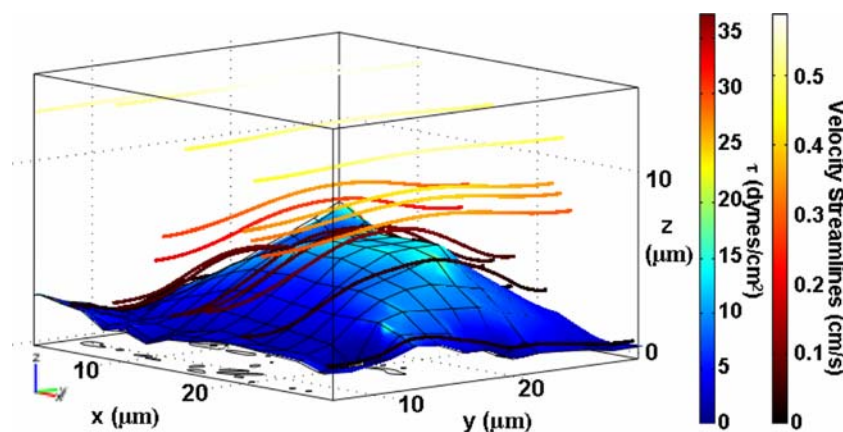


FIGURE 3. Representative subcellular shear stress distribution: a nominal shear stress of 10 dynes/cm^2 was simulated over the solid cell monolayer model in the positive y -direction. Stress distributions show stress peaks at the apical region over the nucleus while stress is minimum in the valleys between cells. Simulated cell represents a single cell in a monolayer. Simulated velocity field is shown using streamlines. Color plot of shear stress in dynes/cm^2 ; streamline color corresponds to fluid velocity (cm/s). Axes in μm .

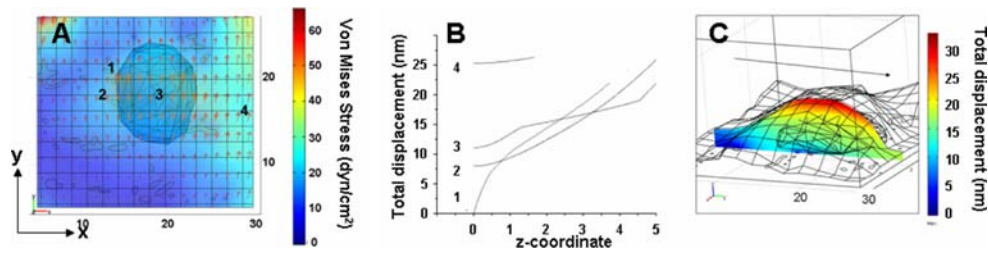


FIGURE 4. (A) Shear-induced cell deformation. Deformation (nm) color plot with deformation direction shown in red arrows. Red arrows are a maximum projection of all deformation arrows plotted as a function of the z -coordinate. Arrows are proportional to deformation but have been scaled to make them visible. Axes in μm , deformation color plot in nm. (B) Shear-induced cell deformation as a function of distance from the glass substrate (z -coordinate). Deformation was plotted as a function of z -coordinate for focal adhesions 1–4 denoted by the numbers in A. Note that location 1 corresponds to a focal adhesion and therefore has a zero displacement at $z = 0$. Deformations are only plotted for z -positions for which data exists (inside the simulated cell). (C) Representative yz slice (same as used in Fig. 5B,C) showing displacement map. Arrow denotes apical flow direction. Color plot in nm.

attachment locations introduced heterogeneity in deformation direction which differed from those in the uniformly fixed base case (not shown). Model predictions of deformations of a focally-adhered endothelial cell were largely determined by the number, density, and size of adhesions (Fig. 4). For example, z -dependent deformations over FAs ranged from 0 nm at the base to 25 nm at the cell surface (point 1 Fig. 4A, B) while deformations ranged from 20 nm at the base to 25 nm at the surface in areas where there were few FAs (point 4 Fig. 4A, B). Deformation was minimal in the basal region and increased with increasing distance away from glass substrate (Fig. 4B). Maximal deformation of the cell in the center of the simulation space was ~ 30 nm (Fig. 4C).

The addition of FAs as attachment locations for the cell also had an effect on the internal strains (Fig. 5). Considering normal strain in the z -direction, FAs introduced heterogeneity in strains, which were concentrated close to the FAs and propagated away. As an example, a color plot of z -normal strain (e_{zz}) evaluated at a height of 100 nm above the glass surface is displayed in Fig. 5A. This height was chosen to put the plane of analysis close to the base of the cell but entirely in the cytoplasm. With the inclusion of FAs as attachment points, the peak strains were larger by nearly an order of magnitude compared to the case of a uniformly fixed base (not shown). There was observable strain focusing at the edges of the adhesion

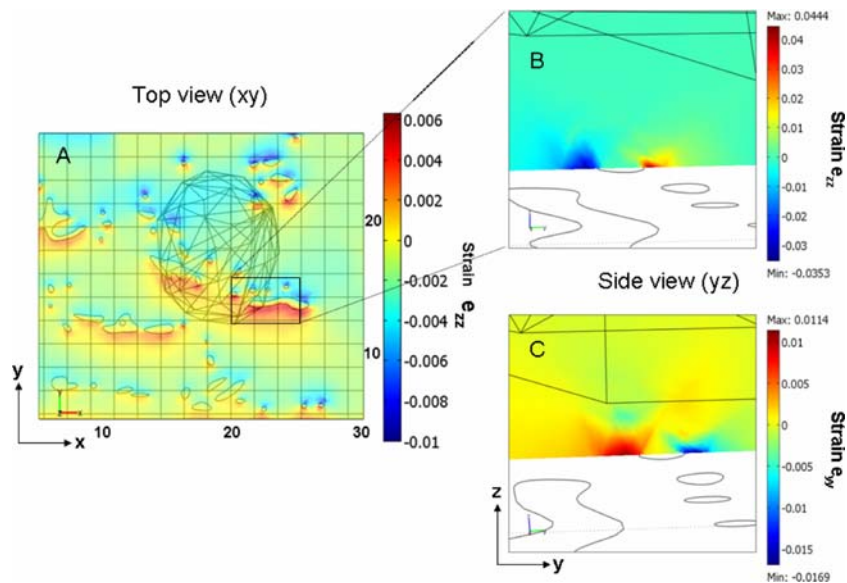


FIGURE 5. Effects of focal adhesions on shear-induced strain. Flow is in the positive y -direction and is applied to the apical surface of the cell. Axes in microns. Negative strains are compressive and positive strains are tensile. Color plot legend denotes strain magnitudes (e.g. 0.006 = 0.6% strain). (A) Strain in the z -direction (e_{zz}) evaluated at $z = 0.1 \mu\text{m}$ above the coverslip. (B) A slice plot for e_{zz} along a yz plane at $x = 20 \mu\text{m}$. Image has been zoomed and turned to observe strain focusing near focal adhesion which propagates into cytoplasm. (C) Similar to B except that strain in the y -direction (e_{yy}) has been computed. Values in C suggest compressive and tensile e_{yy} strains in the upstream and downstream portions of the focal adhesion, respectively.

sites. The trend for e_{zz} was compressive and tensile on the upstream and downstream edge of the FA, respectively (Fig. 5B) while e_{yy} , was compressive on the upstream and tensile on the downstream portion (Fig. 5C). The terms upstream and downstream were chosen to be consistent with the flow direction (upstream to downstream). These strain concentrations tended to propagate outward from their origins on the FAs and diminish with increasing distance from the coverglass. Nevertheless, maximum internal strains resulting from a nominal surface shear stress of 10 dynes/cm² were predicted to range from 1 to 4%. Plots of cell-scale principle stresses and strains revealed a general trend of tensile stress in the cytoplasm on the side upstream of the nucleus and compressive stresses in the downstream side (not shown).

To determine the relationship between FA area and strain, two models were solved and strains near FAs were computed. The maximum and minimum strains (found immediately adjacent to FAs) in the y - and z -directions were then plotted and fit with a linear function. Results (Fig. 6) of curve fitting provide estimates of maximum and minimum strains for FAs of arbitrary area.

With respect to stresses, the inclusion of FAs induced substantial stress amplification and focusing (Fig. 7A). For example, maximal von Mises stress was 380 dynes/cm², a 38-fold increase over the nominal

shear stress at the surface (Fig. 7B). When the model was solved without FAs, maximal stresses were on the order of 30 dynes/cm² and mirrored the surface shear stress distribution (Fig. 7A). FA-amplified stresses were directional with large compressive stresses in the y -direction upstream of the FA and large tensile stresses downstream. When the model was solved with the nucleus, stresses near FAs under the nucleus were about 30% less than when the model was solved without the nucleus (not shown).

Material Inhomogeneities and Nucleus-Induced Stress Amplification

The model was constructed to determine the role of the high-modulus nucleus on internal cellular stresses and strains. When the modulus of the nucleus was artificially set equal to the cytoplasmic modulus of 774 Pa, (effectively negating the effect of the nucleus without changing mesh settings), the von Mises stress evaluated at 2.5 μm from the base was nearly uniform and ranged from ~ 20 to 30 dynes/cm² (Fig. 8A). When the nuclear modulus was set equal to the experimentally measured modulus of 5,100 Pa, stresses at 2.5 μm from the base ranged from 40 to 60 dynes/cm² (Fig. 8B). These higher stresses were located exclusively in the nucleus near the nucleus–cytoplasm interface. Stresses elsewhere in the cytoplasm were more uniform and on the order of 20–30 dynes/cm².

The high-modulus nucleus also affected strain distributions in the cytoplasm and nucleus. For example, at the interface with the nucleus, cytoplasmic strains were on the order of 0.05–0.1% when the nucleus was not included and increased moderately to 0.2% when it was included (Fig. 8C, D). More significantly, the high nuclear modulus resulted in shielding of the nucleus from high strains. In other words, although stresses were concentrated in the nucleus, strains were $< 0.05\%$.

Focal Adhesions Result in Stress Heterogeneities in Response to Bead Twisting

Magnet-induced rotation of integrin-attached ferromagnetic beads induces pN-loading of cell surfaces which has been successfully modeled using finite element analysis.^{35,38} Such rotation results in mitochondrial displacements and stress focusing approximately 1 μm above the cell base and far from the loading source.²⁵ Stress focusing refers to the areas where high stresses are spatially confined and surrounded by lower stresses. In this study, we sought to determine if the presence of FAs could lead to stress focusing in the cell interior. Thus, we modeled

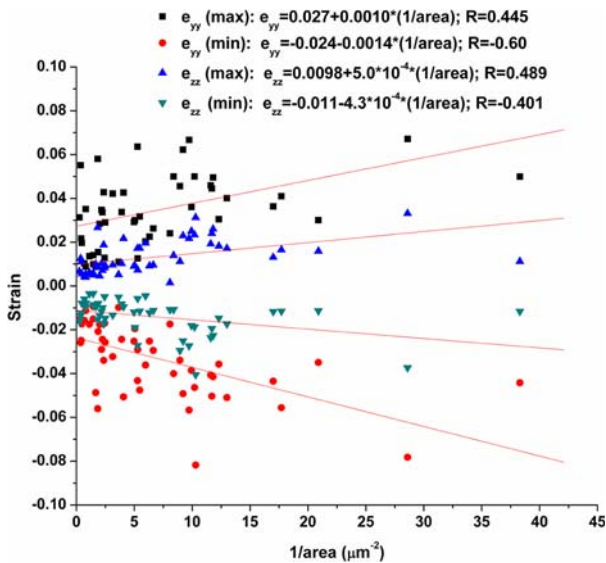


FIGURE 6. Relationship between strains near focal adhesions and FA area. Maximum and minimum e_{yy} and e_{zz} strains located immediately adjacent to focal adhesions were plotted against the reciprocal of focal adhesion area for two models of multicomponent, confluent endothelial cells. Positive and negative strains are tensile and compressive, respectively. Legend indicates linear fit according to $e_{ij} = b + m \cdot (1/\text{area})$ and correlation coefficients, R . Total number of FAs analyzed was 50.

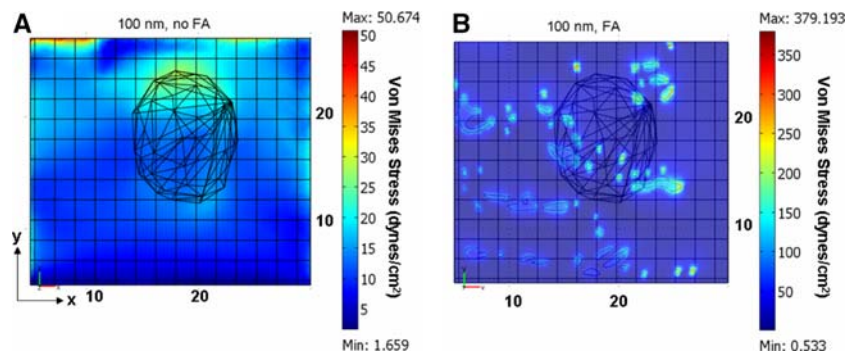


FIGURE 7. Effects of focal adhesion on shear-induced stresses. von Mises stress distributions were evaluated at $z = 0.1 \mu\text{m}$ above the coverslip for (A) model computed without focal adhesions and (B) model solved with focal adhesions.

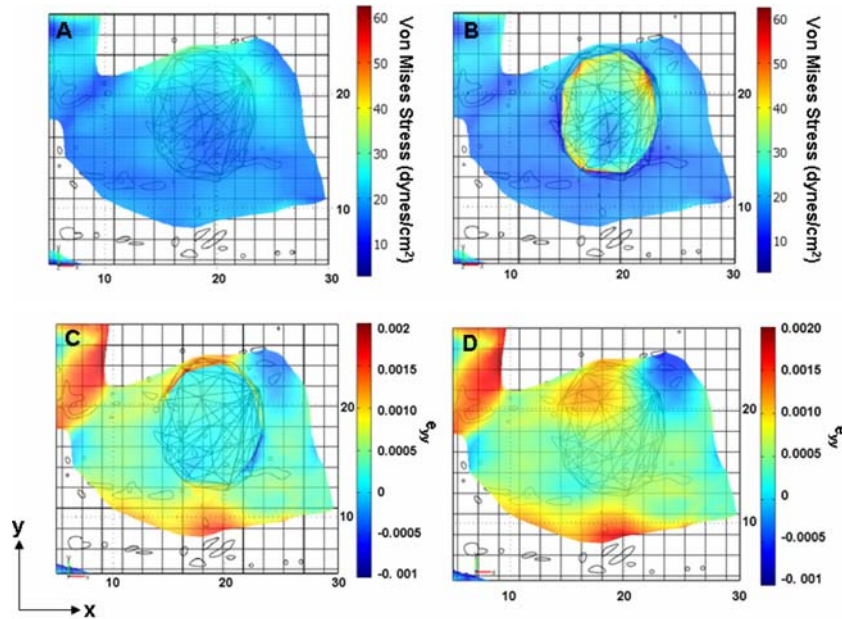


FIGURE 8. Effects of nucleus on shear-induced stresses and strains. (A) von Mises stress distribution for a model in which the nuclear modulus was set equal to the cytoplasmic modulus (774 Pa) in order to neglect the effects of the nucleus without altering mesh conditions. Note uniformity of stresses in the vicinity of the nucleus. (B) von Mises stress distribution for a model solved with the nuclear modulus equal to 5,100 Pa (actual modulus). Note that the stiffer nucleus induced local high stress concentrations in the nucleus–cytoplasm interface. (C) e_{yy} strains with nucleus. (D) e_{yy} strains without nucleus. e_{yy} strains were larger than those in x and z directions and larger than shear strains.

the response of the cell to 20° rotation of a $1 \mu\text{m}$ bead embedded and mechanically coupled $\sim 50\%$ into the cell surface. The predicted displacement map exhibited maximum total displacements near the bead which fell off rapidly with increasing distance (Fig. 9C). At $1 \mu\text{m}$ above the cell surface, bead rotation induced heterogeneity of displacement in focally adhered ECs but not in cells uniformly attached at the base (Fig. 9C, D). Lower displacements occurred in areas near FAs. Similarly, maps of von Mises stress at $z = 1 \mu\text{m}$ exhibited increased heterogeneity of stress distribution (Fig. 9A,B). Importantly, focused stresses were predicted above

FAs far from the bead. These same stress concentrations were not predicted when the cell base was uniformly constrained.

DISCUSSION

This study provides the first quantitative predictions of stress distributions in focally adhered ECs resulting from apically applied fluid-flow. These results arise from finite-element analysis of a cell-specific model in which surface topography and FA location and area were experimentally determined. The model predicts

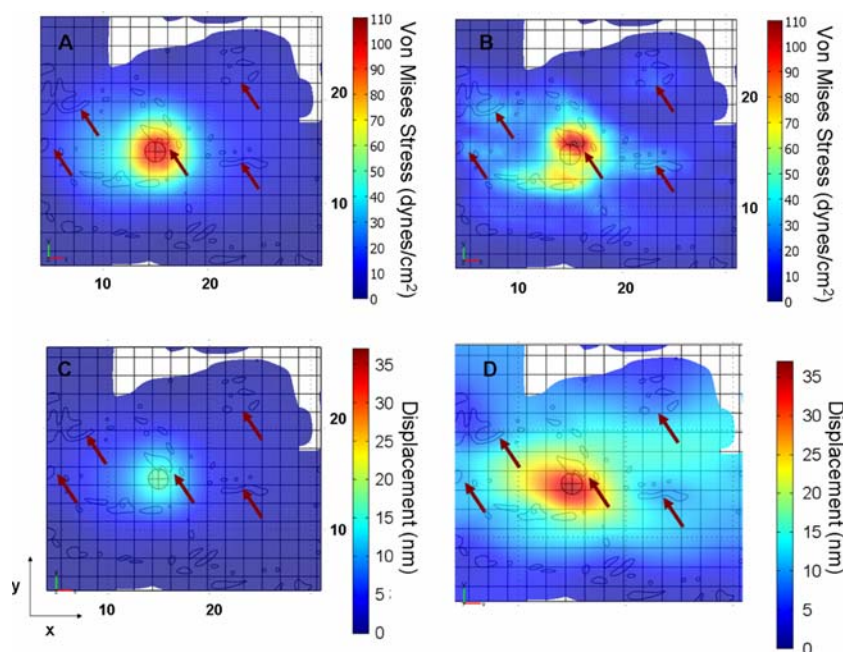


FIGURE 9. Stresses and displacements computed at $1\ \mu\text{m}$ above base in solid model with 20° rotation about y -axis of a bead embedded 50% into cell. Arrows denote areas of stress focusing in B. (A) von Mises stress distribution (dynes/cm^2) due to bead rotation in model without focal adhesions. (B) von Mises stress distribution (dynes/cm^2) due to bead rotation in model with focal adhesions. (C) Deformation (nm) due to bead rotation in model without focal adhesions. (D) Deformation (nm) due to bead rotation in model with focal adhesions. Color bar represents deformation (nm). Axes in μm .

that shear-induced stresses were generally small but significantly amplified and focused near FAs and the high-modulus nucleus.

Effects of FAs on Distributions of Stress, Strains, and Displacements

Inclusion of FAs as attachment locations in a homogeneous linear elastic continuum model resulted in heterogeneous internal stresses, strains, and displacements. Stresses near FAs were nearly 40-fold larger than surface shear stresses thus supporting the widely held contention that FAs are a means of force amplification of shear stress. Shear stress induced cytoplasmic displacements that were small near FAs and larger in areas absent FAs. Strains were largest in the vicinity of FAs and diminished with increasing distance away from FAs. Although inclusion of FAs resulted in larger deformations compared to a uniformly constrained base, deformations from shear stress were still small ($<100\ \text{nm}$). While deformation due to applied stress is dependent on the modulus used in the simulation, the 2-fold range of moduli reported in the literature⁸ would affect deformation results only by a factor of 2 at most. Deformations from the bead-twisting model were comparable to those observed by Hu and colleagues at early times

after force imposition.²⁵ In addition, the magnitude of the displacements predicted by our model are consistent with rapid (1–10 s) displacements seen in endothelial cells as determined from the tracking of endogenous particles in the cytoplasm (unpublished observations). Thus the present model provides quantitative predictions of early, rapid, shear-induced deformations (which are important in the earliest mechanotransduction events). Larger force-induced displacements of cytoplasmic components^{20,23} observed on the order of minutes to hours after shear-imposition may be better explained by models which include structural remodeling, plastic deformation, or cytoskeletal force generation.

Effects of Material Inhomogeneities on Stress Distributions

Composite materials made of stiff and soft structures, when stressed, exhibit stress concentrations in and around the stiff structure. Consistent with this principle, we quantified stress amplification near the high-modulus nucleus. While overall strains were small ($\sim 0.5\%$) inclusion of the nucleus in the model increased peri-nuclear strains that were 2-fold greater than the case when the nucleus was not included in the model. Similarly, stresses in the nucleus were large

(~ 50 dynes/cm²) although strains were low ($\sim 0.05\%$). Deguchi *et al.* recently found that shear stress leads to an increased in nuclear stiffness while our analysis suggests that stresses are high in the nucleus and strains are high in the soft cytoplasm.¹³ Thus it is possible that nuclear mechanical properties are regulated by intranuclear stresses transmitted from the cell surface to the nucleus. Jean *et al.* showed that stresses can be transmitted to the nucleus during cell rounding and spreading.^{28,29} In that study, it was suggested that forces transmitted to the nucleus may be sufficient to alter gene expression directly. However, stresses transmitted to the nucleus as a result of apical fluid flow are likely to be less than those resulting from cell contraction. Thus, it is unclear whether shear stress can transmit sufficient stresses to the nucleus for direct mechanotransduction of gene expression.

Cytoplasmic Stresses Resulting from Alternative Forcing Functions

Heterogeneous, focused displacements in response to bead rotation predicted by our model are consistent with experimental observations reported by Hu and colleagues but inconsistent with their simplified continuum elastic model of bead twisting.²⁵ The discrepancies between these models are due to the fact that the simplified model did not include actual cell topography, a high-modulus nucleus, or FAs. In support of the role of FAs in anisotropic mechanical behavior Hu and colleagues showed that disruption of stress fibers reduced but did not eliminate the mechanical anisotropy deduced from a novel 3-D cellular magneto-rheometer.²⁶ Thus, FAs, in addition to stress fibers, may be important origins of stress focusing in cells while stress fibers may be necessary to explain the “action at a distance” observed in Hu *et al.* and predicted by tensegrity theory.⁴⁶ The observations from the present study, therefore, support the use of a homogenous, isotropic continuum to predict a heterogeneous mechanical response to external loading in living endothelial cells provided focal attachment points are accurately modeled.

Our model predicts that high stresses are correlated with small displacements near FAs. Thus large strains (and stress) will occur in areas where constrained regions and free regions are juxtaposed, such as above FAs (shown in Fig. 9). This observation may explain experimental observations in a recent study in which caveolin- and integrin-mediated signaling in response to shear stress were co-localized.^{18,41}

Comparisons of displacements and stresses in the cytoplasm also suggest that stresses and displacements resulting from bead twisting are comparable to those from shear stress, although the directions of the effects

differed between the two forcing modalities. When our model was solved for 0.9 nN lateral pulling on an embedded bead, deformations near the bead on the order of 1 μm were predicted (not shown) suggesting that bead pulling does not replicate shear-induced apical membrane displacements. However, stresses near the base of the cell from the bead twisting and pulling were comparable to those resulting from shear stress, a finding consistent with Ref. 34.

Modeling of the Surface Glycocalyx

Endothelial cells are known to have a carbohydrate and plasma protein-rich surface glycocalyx the dimensions of which depend on media composition.¹ This layer may affect some aspects of mechanosensing by modulating the transfer of shear stress to the cell membrane or cytoplasm.^{36,48,49} Although the presence or properties of the glycocalyx were not experimentally assessed in this study, we can estimate the effects of the glycocalyx on overall fluid drag on the cell using a model proposed by Weinbaum *et al.*⁵⁵ In their calculations the glycocalyx was considered a 0.4 μm thick poroelastic Brinkman layer (for flow through porous media) mechanically coupled to the apical membrane. The Brinkman velocity, \mathbf{u}_b , was determined from:

$$\eta \nabla^2 \mathbf{u}_b = \left(\frac{\eta}{K_p} \mathbf{u}_b + \nabla p \right) \quad (7)$$

$$\nabla \cdot \mathbf{u} = 0$$

where the second equation is the continuity equation. Fluid drag from the NS domain on the solid portion of the Brinkman layer was estimated by computing the forces on idealized vertical strands with N strands/unit area (Eq. 3 from⁵⁵):

$$F(r) = \frac{\pi \eta U(r) r^2}{c K_p} \quad (8)$$

$$c = \frac{2\pi r_f^2}{\sqrt{3}(2r_f + \Delta)}$$

where $F(r)$ is force on a strand as a function of distance, r , from the membrane, $U(r)$ is the local (Brinkman) velocity, r_f is the radius of a strand (6 nm), c is the fiber volume fraction (calculated as 0.326), K_p is the Brinkman permeability (3.157×10^{-18} m²), and Δ is the inter-strand spacing (8 nm). If each strand is centered on a vertex of an equilateral triangle with sides of length $2r_f + \Delta$, one can estimate the number of strands per area to be approximately 2.89×10^{15} strands/m². After integrating the velocity along the strand and calculating the overall drag/strand from Eq. 8, the drag force is 7×10^{-4} pN/strand for the nominal shear stress of 10 dynes/cm².⁵⁵ This drag on an individual strand

results in an overall drag on the cell (pN/strand*stands/area) of 20.0 dynes/cm². If the top surface of the glycocalyx was subjected to all of the shear stress, then mechanical equilibrium would dictate that the overall drag on the cell would be the same with or without the glycocalyx. However, because of increased surface area contributed by vertical strands, and the transmission of flow from the free stream to the upper surface of the Brinkman layer, overall drag is increased by a factor of ~ 2 . Inclusion of the glycocalyx in our model would increase stresses and strains by this factor. It can be seen from this analysis that the presence of a glycocalyx may constitute an important additional mechanism for stress amplification in vascular endothelial cells. It should be pointed out, however, that much about the glycocalyx is unknown and its role in mechanotransduction is controversial. For example, recent studies suggest that the glycocalyx is important for some aspects of mechanotransduction and not for others.^{16,42} However, from our analysis, it is suggested that experiments which denude endothelial cells of the glycocalyx or experiments which fail to use plasma components in the perfusates, may unintentionally alter the stress distribution in the cell and at FAs.

Limitations of Isotropic Linear Elasticity

Linear elasticity is a known limitation of our model. Since the time constant for viscoelasticity of endothelial cells is estimated to be ~ 1 s,³⁰ the results of the present model represent the deformation at early times after viscous damping can be neglected. Similarly, active remodeling of actin (and mechanical properties) in response to shear stress may occur as early as 5 min after shear onset. Therefore, the estimates of stress and strain distributions presented here should be used to interpret very early mechanotransduction events.

Cells are known to contain a meshwork of microtubules and filaments which can transmit mechanical loads from the cell surface to the interior.²⁰ However, it has been shown here that a continuum approach to cell mechanics can reproduce heterogeneous response in cells consistent with what is reported in the literature, suggesting that the cytoskeletal structures and other organelles are sufficiently inter-connected and pore sizes are small enough (~ 50 nm) for the cytoplasm to be approximated by continuum theory. However, interconnections of stiff filaments and compressive elements may play a role in altering the transmission of stress within the cell.⁵³ A very stiff filament may act as a stress isolator when the cell is in tension. In this case a continuum model which neglects this stress isolator would over-estimate stress transmission from the apical surface to the base. In other cases, stiff compressive elements might enhance stress transmission and a

continuum model would thus underestimate stresses near the base. Importantly, it has been shown that the modeling techniques employed here have the potential to model internal cell structures (e.g. nucleus). As computing power increases, the potential of these techniques to model structures with finer detail increases. In the future, it will become desirable to counter-stain for additional internal structures such as microtubules, stress fibers, and intermediate filaments and include them in a multicomponent continuum model. However, although computational limitations motivate the use of a continuum approach, it is likely that the complete architectural structures which contribute to cell mechanics could not be modeled accurately with discrete representations of the structures and their interactions. Thus, a continuum model may lead to more accurate predictions of stress transmission due to the inherent representation of all relevant internal structures. An alternative approach to imaging the all cytoskeletal elements is to measure mechanical properties in many locations of the same cells being simulated to create a heterogeneous continuum elastic solid model of the cell.⁸

Effects of Imaging Uncertainties on Model Predictions

The solid modeling procedures developed here use surface topographies and mechanical properties which have inherent uncertainty. First, since the detection of cell edges is determined by a user-selected threshold, altering this value can induce slight changes in the final structure produced by the modeling program. This uncertainty is minimized by image deconvolution which makes the edges more obvious by reduction of blur. In addition, axial distortions inherent in biological imaging were minimized using an axial distortion correction function resulting in similar surface shear distributions as those computed when the surface was measured with atomic force microscopy.²

Second, it is possible that TIRFM does not reveal all attachment points of the cell and or the true size and shape of FAs. To address these issues, we used TIRFM to image cells transfected with green fluorescent protein-tagged focal adhesion kinase (GFP-FAK) as a counter-stain to calcein (a red shifted version). We found that most GFP-FAK-positive FAs were detected by quantitative TIRF and had similar shapes and areas. Those areas which were attached to the glass but not GFP-FAK positive were likely not mature adhesions. However, it is appropriate to consider these areas as attached with respect to model development. Although GFP-FAK provides excellent single-to-noise ratios, TIRFM of calcein-stained cells makes feasible the reproduction of basal membrane topography, which would be useful in developing a

microscale model of basal cell mechanics in response to apically applied stresses.

Prestress in Cells

Endothelial cells exhibit contractility under static conditions⁴⁰ suggesting that cells are stressed internally. Due to the large number of filaments in the cell, it would be difficult to account for prestress in each filament and incorporate it into a holistic model. Alternative methods of applying prestress to a continuum include use of an estimated uniform prestress or assignment of directional prestress at individual FAs. Applications of a uniform physiological prestress in the current model yielded slight changes in magnitude of stress in sheared ECs but had only marginal effects on stress distributions (data not shown). Pourati and colleagues demonstrated that prestress increases endothelial cell stiffness in response to eternally applied forces.⁴⁰ In their study, stiffness increased by about 10 and 25% in response to 2.5 and 5% strain applied at the surface, respectively. These strains are much larger than the surface strains predicted in our model in response to 10 dynes/cm² surface shear stress. Thus the increases in modulus due to physiological shear and EC prestress are likely to be well below 10% and have only modest effects on shear-induced deformation.

Relationship Between Stress and Endothelial Cell Mechanotransduction

Mechanotransduction is the process by which cells convert mechanical stimuli into intracellular chemical signaling cascades. Mechanotransduction is known to be involved in the regulation of homeostasis of many tissues including the vascular endothelium.¹¹ Interest in the precise mechanisms by which endothelial cells sense and respond to mechanical signals arises from a now well-established correlation between spatial and temporal variations in hemodynamic shear stress and the focal nature of atherosclerotic lesions. Candidate cellular structures responsible for mechanotransduction in ECs include FAs, plasma membrane subdomains,^{4,43} cell-cell junctions,⁵² and others.

It has not yet been shown, however, that physiological shear stress results in sufficient stress in these regions to directly activate signaling. In order to better understand force transmission in single cells, finite element mechanical approaches deal effectively with complex geometries and force impositions^{8,30} and provide good approximations of force levels in idealized cells and in cells in which topography and mechanical properties have been measured. In support

of the use of continuum theory in mechanotransduction, Mack and co-authors used FEA of an idealized cell subject to point deformation from a magnetic bead to correlate the stresses in FA to FA translocation as determined by fluorescence images of GFP-paxillin, a protein that binds to FAK in mature FAs. Similarly, Charras and colleagues demonstrated that FEA-predicted stresses correlated well with ion channel opening in bone cells.⁹

While it is difficult to couple information from a continuum model to forces on individual molecules, Charras and Horton recently showed that stresses and strains resulting from fluid shear stress are below the threshold needed to activate candidate shear-sensitive molecules.⁸ However, because their model did not include the nucleus or FAs, they could not predict the stress-amplification mechanisms suggested in our study. In our model, strains on the order of 1–4% are predicted. If these strains were applied to the membrane near FAs, it is conceivable that transmembrane proteins could be activated there.

It is possible that cell-cell junctions¹⁹ are additional mechanisms of force amplification. A recent report by Tzima and colleagues suggests that PECAM-1, along with adapter molecules may constitute a force-sensitive system which indirectly activates integrin molecules.⁵² In that study, both shear stress and bead pulling were used as forcing functions to activate integrins in endothelial cells. Since cell junctions were not explicitly included in the present model, it is not yet clear that bead pulling and shear stress elicit comparable stresses at cell junctions. Our study focused on cellular stresses in response to apically applied fluid shear stress in order to begin to evaluate extant theories on focal-adhesion-mediated mechanotransduction of fluid shear stress. It is possible that other modes of force (e.g. cell contraction, substrate stretching, bead pulling) may stimulate different molecular signaling pathways than those activated by fluid shear stress.⁸

Cell-Specific Stress Analysis and Mechanotransduction

In summary, this study presents the first estimates of heterogeneous displacements and stress-strain fields in sheared and focally-adhered endothelial cells. These heterogeneous stress responses are due to the inclusion in the model of distributed attachment locations (i.e. FAs) and cellular components with different elastic moduli. The location and directions of upstream tensile and downstream compressive stresses computed in the vicinity of individual FAs were consistent with the observation of FA growth in the downstream direction of flow and FA retraction

in the upstream side, thus providing needed quantitative information to elucidate mechanisms of mechanotaxis of ECs.^{12,33,56} Further work is necessary to extract stresses from individual FAs and to precisely compute forces on integrin-extracellular matrix bonds to evaluate integrin-mediated force sensing. If such modeling methods are followed by cellular probing for physiological changes and molecular signaling events on the same cells, direct correlations could be made between sub-cellular stresses and signaling (i.e. cell-specific mechanotransduction) to assess which structures are the dominant mechanotransducers under physiological and pathophysiological conditions. Elucidating molecular mechanisms of alterations in EC phenotypes from atheroprotective to atherogenic in response to prevailing wall shear stress is an important component of the development of therapeutic interventions in vascular disease.

In order to determine the precise molecular mechanisms which couple force and biochemical signaling in ECs, it is useful to combine engineering analysis of intact endothelial cells with real-time experimental readouts of the same cell using comparable spatial and temporal scales; in other words, cell-specific models constructed from accurate input parameters of cell topographies and boundary conditions followed by micron-scale interrogation of molecular changes in areas of stress or strain focusing. Such analysis would lead to direct, same-cell correlation of experimental measurements and stress distributions. While atomic force microscopy (AFM) and electron microscopy (EM) can yield ultra-high-resolution topographies for solid models, fluorescence microscopy can yield high-resolution images of surface and internal cellular features of viable cells. In addition to yielding insight into the role of surface topography, nuclei, and FAs in shear-induced stress distributions, these methodologies set the stage for cell-specific modeling and experimentation to elucidate the fundamental mechanisms of mechanotransduction.

ACKNOWLEDGMENTS

This work was supported in part by a grant to PJB from the National Heart Lung and Blood Institute (R01 HL 077542-01A1), by a National Science Foundation Career Award to PJB (BES 0238910), and by a seed grant from the Center for Optical Technologies, Bethlehem, PA. GFP-FAK was a gift from Song Li, Ph.D., University of California, Berkeley. MBG was supported by the Penn State Biomaterials and Bionanotechnology Summer Institute (NIBIB-NSF EEC 0234026).

REFERENCES

- ¹Adamson, R. H. and G. Clough. Plasma proteins modify the endothelial cell glycocalyx of frog mesenteric microvessels. *J. Physiol.* 445:473–486, 1992.
- ²Barbee, K. A., T. Mundel, R. Lal and P. F. Davies. Subcellular distribution of shear stress at the surface of flow-aligned, nonaligned endothelial monolayers. *Am. J. Physiol. Heart Circ. Physiol.* 268:H1765–H1772, 1995.
- ³Bursac, P., G. Lenormand, B. Fabry, M. Oliver, D. A. Weitz, V. Viasnoff, J. P. Butler and J. J. Fredberg. Cytoskeletal remodelling, slow dynamics in the living cell. *Nat. Mater.* 4:557–561, 2005.
- ⁴Butler, P. J., G. Norwich, S. Weinbaum and S. Chien. Shear stress induces a time-, position-dependent increase in endothelial cell membrane fluidity. *Am. J. Physiol. Cell Physiol.* 280:C962–C969, 2001.
- ⁵Butler, P. J., T. C. Tsou, J. Y. Li, S. Usami, and S. Chien. Rate sensitivity of shear-induced changes in the lateral diffusion of endothelial cell membrane lipids: A role for membrane perturbation in shear-induced MAPK activation. *FASEB J.* 16(2):216–218, 2001.
- ⁶Butler, P. J., S. Weinbaum, S. Chien and D. E. Lemons. Endothelium-dependent, shear-induced vasodilation is rate-sensitive. *Microcirculation* 7:53–65, 2000.
- ⁷Caille, N., O. Thoumine, Y. Tardy and J. J. Meister. Contribution of the nucleus to the mechanical properties of endothelial cells. *J. Biomech.* 35:177–187, 2002.
- ⁸Charras, G. T. and M. A. Horton. Determination of cellular strains by combined atomic force microscopy, finite element modeling. *Biophys. J.* 83:858–879, 2002.
- ⁹Charras, G. T., B. A. Williams, S. M. Sims and M. A. Horton. Estimating the sensitivity of mechanosensitive ion channels to membrane strain, tension. *Biophys. J.* 87:2870–2884, 2004.
- ¹⁰Charras, G. T., J. C. Yarrow, M. A. Horton, L. Mahadevan and T. J. Mitchison. Non-equilibration of hydrostatic pressure in blebbing cells. *Nature* 435:365–369, 2005.
- ¹¹Davies, P. F., Flow-mediated endothelial mechanotransduction [Review] [407 refs]. *Physiol. Rev.* 75:519–560, 1995.
- ¹²Davies, P. F., A. Robotewskyj and M. L. Griem. Quantitative studies of endothelial cell adhesion. Directional remodeling of focal adhesion sites in response to flow forces. *J. Clin. Invest.* 93:2031–2038, 1994.
- ¹³Deguchi, S., K. Maeda, T. Ohashi and M. Sato. Flow-induced hardening of endothelial nucleus as an intracellular stress-bearing organelle. *J. Biomech.* 38:1751–1759, 2005.
- ¹⁴DePaola, N., M. A. Gimbrone Jr., P. F. Davies and C. F. Dewey Jr., Vascular endothelium responds to fluid shear stress gradients. *Arterioscler. Thromb.* 12:1254–1257, 1992.
- ¹⁵Ferko, M. C., B. P. Patterson and P. J. Butler. High-resolution solid modeling of biological samples imaged with 3D fluorescence microscopy. *Microsc. Res. Tech.* 69(8):648–655, 2006.
- ¹⁶Florian, J. A., J. R. Kosky, K. Ainslie, Z. Pang, R. O. Dull and J. M. Tarbell. Heparan sulfate proteoglycan is a mechanosensor on endothelial cells. *Circ. Res.* 93:e136–e142, 2003.
- ¹⁷Frangos, J. A., T. Y. Huang and C. B. Clark. Steady shear, step changes in shear stimulate endothelium via independent mechanisms-superposition of transient and sustained nitric oxide production. *Biochem. Biophys. Res. Commun.* 224:660–665, 1996.
- ¹⁸Frank, P. G. and M. P. Lisanti. Role of caveolin-1 in the regulation of the vascular shear stress response. *J. Clin. Invest.* 116:1222–1225, 2006.

- ¹⁹Fujiwara, K., M. Masuda, M. Osawa, Y. Kano and K. Katoh. Is PECAM-1 a mechanoresponsive molecule?. *Cell Struct. Funct.* 26:11–17, 2001.
- ²⁰Galbraith, C. G., R. Skalak and S. Chien. Shear stress induces spatial reorganization of the endothelial cell cytoskeleton. *Cell Motil. Cytoskeleton* 40:317–330, 1998.
- ²¹Gudi, S. R., C. B. Clark and J. A. Frangos. Fluid flow rapidly activates G proteins in human endothelial cells. Involvement of G proteins in mechanochemical signal transduction. *Circ. Res.* 79:834–839, 1996.
- ²²Haidekker, M. A., N. L'Heureux and J. A. Frangos. Fluid shear stress increases membrane fluidity in endothelial cells: A study with DCVJ fluorescence. *Am. J. Physiol. Heart Circ. Physiol.* 278:H1401–H1406, 2000.
- ²³Helmke, B. P., R. D. Goldman and P. F. Davies. Rapid displacement of vimentin intermediate filaments in living endothelial cells exposed to flow. *Circ. Res.* 86:745–752, 2000.
- ²⁴Helmke, B. P., A. B. Rosen and P. F. Davies. Mapping mechanical strain of an endogenous cytoskeletal network in living endothelial cells. *Biophys. J.* 84:2691–2699, 2003.
- ²⁵Hu, S., J. Chen, B. Fabry, Y. Numaguchi, A. Gouldstone, D. E. Ingber, J. J. Fredberg, J. P. Butler and N. Wang. Intracellular stress topography reveals stress focusing, structural anisotropy in cytoskeleton of living cells. *Am. J. Physiol. Cell Physiol.* 285:C1082–C1090, 2003.
- ²⁶Hu, S., L. Eberhard, J. Chen, J. C. Love, J. P. Butler, J. J. Fredberg, G. M. Whitesides and N. Wang. Mechanical anisotropy of adherent cells probed by a three-dimensional magnetic twisting device. *Am. J. Physiol. Cell Physiol.* 287:C1184–C1191, 2004.
- ²⁷Jalali, S., M. A. del Pozo, K. Chen, H. Miao, Y. Li, M. A. Schwartz, J. Y. Shyy and S. Chien. Integrin-mediated mechanotransduction requires its dynamic interaction with specific extracellular matrix (ECM) ligands. *Proc. Natl. Acad. Sci. USA* 98:1042–1046, 2001.
- ²⁸Jean, R. P., C. S. Chen and A. A. Spector. Finite-element analysis of the adhesion-cytoskeleton-nucleus mechanotransduction pathway during endothelial cell rounding: axisymmetric model. *J. Biomech. Eng.* 127:594–600, 2005.
- ²⁹Jean, R. P., D. S. Gray, A. A. Spector and C. S. Chen. Characterization of the nuclear deformation caused by changes in endothelial cell shape. *J. Biomech. Eng.* 126:552–558, 2004.
- ³⁰Karcher, H., J. Lammerding, H. Huang, R. T. Lee, R. D. Kamm and M. R. Kaazempur-Mofrad. A three-dimensional viscoelastic model for cell deformation with experimental verification. *Biophys. J.* 85:3336–3349, 2003.
- ³¹Koller, A. and G. Kaley. Endothelial regulation of wall shear stress, blood flow in skeletal muscle microcirculation. *Am. J. Physiol.* 260:H862–H868, 1991.
- ³²Laudadio, R. E., E. J. Millet, B. Fabry, S. S. An, J. P. Butler and J. J. Fredberg. Rat airway smooth muscle cell during actin modulation: Rheology, glassy dynamics. *Am. J. Physiol. Cell Physiol.* 289:C1388–C1395, 2005.
- ³³Li, S., P. Butler, Y. Wang, Y. Hu, D. C. Han, S. Usami, J. L. Guan and S. Chien. The role of the dynamics of focal adhesion kinase in the mechanotaxis of endothelial cells. *Proc. Natl. Acad. Sci. USA* 99:3546–3551, 2002.
- ³⁴Mack, P. J., M. R. Kaazempur-Mofrad, H. Karcher, R. T. Lee and R. D. Kamm. Force-induced focal adhesion translocation: Effects of force amplitude, frequency. *Am. J. Physiol. Cell Physiol.* 287:C954–C962, 2004.
- ³⁵Mijailovich, S. M., M. Kojic, M. Zivkovic, B. Fabry and J. J. Fredberg. A finite element model of cell deformation during magnetic bead twisting. *J. Appl. Physiol.* 93:1429–1436, 2002.
- ³⁶Mochizuki, S., H. Vink, O. Hiramatsu, T. Kajita, F. Shigetoto, J. A. Spaan and F. Kajiya. Role of hyaluronic acid glycosaminoglycans in shear-induced endothelium-derived nitric oxide release. *Am. J. Physiol. Heart Circ. Physiol.* 285:H722–H726, 2003.
- ³⁷Nerem, R. M., M. J. Levesque and J. F. Cornhill. Vascular endothelial morphology as an indicator of the pattern of blood flow. *J. Biomech. Eng.* 103:172–176, 1981.
- ³⁸Ohayon, J., P. Tracqui, R. Fodil, S. Fereol, V. M. Laurent, E. Planus and D. Isabey. Analysis of nonlinear responses of adherent epithelial cells probed by magnetic bead twisting: A finite element model based on a homogenization approach. *J. Biomech. Eng.* 126:685–698, 2004.
- ³⁹Olivier, L. A., J. Yen, W. M. Reichert and G. A. Truskey. Short-term cell/substrate contact dynamics of subconfluent endothelial cells following exposure to laminar flow. *Bio-technol. Prog.* 15:33–42, 1999.
- ⁴⁰Pourati, J., A. Maniotis, D. Spiegel, J. L. Schaffer, J. P. Butler, J. J. Fredberg, D. E. Ingber, D. Stamenovic and N. Wang. Is cytoskeletal tension a major determinant of cell deformability in adherent endothelial cells?. *Am. J. Physiol.* 274:C1283–C1289, 1998.
- ⁴¹Radel, C. and V. Rizzo. Integrin mechanotransduction stimulates caveolin-1 phosphorylation recruitment of Csk to mediate actin reorganization. *Am. J. Physiol. Heart Circ. Physiol.* 288:H936–H945, 2005.
- ⁴²Reilly, G. C., T. R. Haut, C. E. Yellowley, H. J. Donahue and C. R. Jacobs. Fluid flow induced PGE2 release by bone cells is reduced by glycocalyx degradation whereas calcium signals are not. *Biorheology* 40:591–603, 2003.
- ⁴³Rizzo, V., A. Sung, P. Oh and J. E. Schnitzer. Rapid mechanotransduction in situ at the luminal cell surface of vascular endothelium, its caveolae. *J. Biol. Chem.* 273:26323–26329, 1998.
- ⁴⁴Sato, M., M. J. Levesque and R. M. Nerem. An application of the micropipette technique to the measurement of mechanical properties of cultured bovine aortic endothelial cells. *J. Biomech. Eng.* 109:27–34, 1987.
- ⁴⁵Sato, M., K. Nagayama, N. Kataoka, M. Sasaki and K. Hane. Local mechanical properties measured by atomic force microscopy for cultured bovine endothelial cells exposed to shear stress. *J. Biomech.* 33:127–135, 2000.
- ⁴⁶Stamenovic, D., N. Wang, and D. E. Ingber. Tensegrity models of cell-substrate interactions. In King, M. R. (ed.) *Principles of Cellular Engineering: Understanding the Biomolecular Interface.* 81–101, 2006.
- ⁴⁷Sund, S. E., J. A. Swanson and D. Axelrod. Cell membrane orientation visualized by polarized total internal reflection fluorescence. *Biophys. J.* 77:2266–2283, 1999.
- ⁴⁸Tarbell, J. M. and M. Y. Pahakis. Mechanotransduction, the glycocalyx. *J. Intern. Med.* 259:339–350, 2006.
- ⁴⁹Thi, M. M., J. M. Tarbell, S. Weinbaum and D. C. Spray. The role of the glycocalyx in reorganization of the actin cytoskeleton under fluid shear stress: A “bumper-car” model. *Proc. Natl. Acad. Sci. USA* 101:16483–16488, 2004.
- ⁵⁰Trickey, W. R., F. P. Baaijens, T. A. Laursen, L. G. Alexopoulos and F. Guilak. Determination of the Poisson's ratio of the cell: Recovery properties of chondrocytes after release from complete micropipette aspiration. *J. Biomech.* 39:78–87, 2006.
- ⁵¹Truskey, G. A., J. S. Burmeister, E. Grapa and W. M. Reichert. Total internal reflection fluorescence microscopy (TIRFM). II. Topographical mapping of relative cell/sub-

- stratum separation distances. *J. Cell Sci.* 103(Pt 2):491–499, 1992.
- ⁵²Tzima, E., M. Irani-Tehrani, W. B. Kiosses, E. Dejana, D. A. Schultz, B. Engelhardt, G. Cao, H. DeLisser and M. A. Schwartz. A mechanosensory complex that mediates the endothelial cell response to fluid shear stress. *Nature* 437:426–431, 2005.
- ⁵³Wang, N., J. P. Butler and D. E. Ingber. Mechanotransduction across the cell surface, through the cytoskeleton. *Science* 260:1124–1127, 1993.
- ⁵⁴Wang, N. and Z. Suo. Long-distance propagation of forces in a cell. *Biochem. Biophys. Res. Commun.* 328:1133–1138, 2005.
- ⁵⁵Weinbaum, S., X. Zhang, Y. Han, H. Vink and S. C. Cowin. Mechanotransduction, flow across the endothelial glycocalyx. *Proc. Natl. Acad. Sci. USA* 100:7988–7995, 2003.
- ⁵⁶Zaidel-Bar, R., Z. Kam and B. Geiger. Polarized downregulation of the paxillin-p130CAS-Rac1 pathway induced by shear flow. *J. Cell Sci.* 118:3997–4007, 2005.